

# A Silicon Micromachined Scanning Thermal Profiler with Integrated Elements for Sensing and Actuation

Yogesh B. Gianchandani, *Member, IEEE*, and Khalil Najafi, *Member, IEEE*

**Abstract**—The thermal profiler is a scanning probe microscope with a miniature thermocouple (TC) at its tip which provides topographic and thermographic information by sensing heat conducted across a small air gap. The silicon micromachined thermal profilers (SMTP's) described in this paper are structurally comprised of a probe that can be longitudinally actuated by an integrated electrostatically driven suspension. A polysilicon-gold TC is located near the probe tip, which overhangs a glass substrate; a resistive heater is integrated with the base. An IC-compatible, 8-mask fabrication process has been developed and SMTP's with various types of frames and probes have been designed, fabricated, and thermally characterized. The maximum thermoelectric signal available from a 7-TC thermopile probe has been measured at 824 mV/W of input power to the heater, whereas from a simpler design it was 48 mV/W. Simple dithered and nondithered scans are presented to demonstrate the basic functionality of fabricated devices. The noise due to our test setup has been measured at  $\approx 20$  mK. For a  $1 \mu\text{m} \times 0.5 \mu\text{m}$  tip and a  $0.1 \mu\text{m}$  long air gap the spatial resolution and the device NETD have been theoretically estimated as  $\approx 3.33$  nm and  $\approx 0.1$  mK/ $\sqrt{\text{Hz}}$ , respectively.

## I. INTRODUCTION

A wide variety of scanning probe microscopes (SPM's) have been developed in the past 15 years based on diverse physical phenomena such as tunneling current, ion conductance, capacitance, force, temperature, light, etc. [1]. The scanning tunneling microscope (STM) and the atomic force microscope (AFM) have found the most widespread use, and are important milestones in the development of SPM's. The spatial resolution achievable by either one of these techniques is  $<1 \text{ \AA}$ , while the operating gap between the tip and the sample is typically  $<10 \text{ \AA}$ . The scanning thermal profiler (STP) interacts with the sample by sensing heat conducted through the scanning probe, and can be used to provide both temperature and topographic information. Although the best reported spatial resolution for it is about an order of magnitude larger than for AFM's and STM's, it permits a wide latitude in the gap size. This is because the thermal interaction between the tip and the sample can exist over a much longer range than tunneling current and near-field forces.

Manuscript received March 29, 1996; revised January 24, 1997. The review of this paper was arranged by Editor M. Fukuma. This work was supported by the National Science Foundation (Awards ECS-8915215 and ECS-9254700) and ARPA (Contract JFBI 92-149).

Y. B. Gianchandani was with the Center for Integrated Sensors and Circuits, University of Michigan, Ann Arbor, MI 48109-2122 USA. He is now with the Department of Electrical and Computer Engineering, University of Wisconsin, Madison, WI 53706-1691 USA.

K. Najafi is with the Center for Integrated Sensors and Circuits, University of Michigan, Ann Arbor, MI 48109-2122 USA.

Publisher Item Identifier S 0018-9383(97)07725-3.

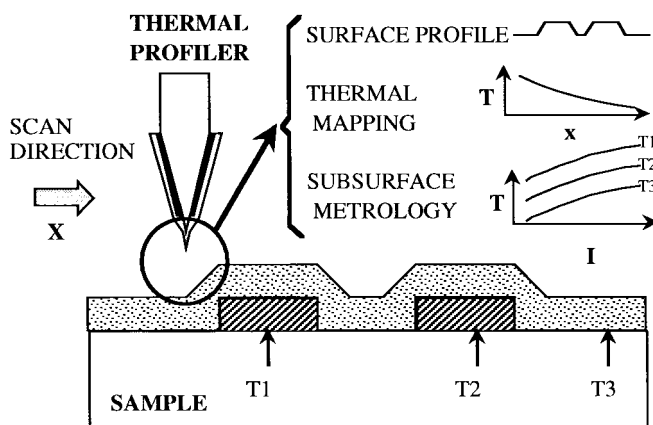


Fig. 1. The scanning thermal profiler uses a sharp thermocouple to sense heat conducted across a small air gap. Applications include topographical mapping, thermal mapping, and photothermal absorption spectroscopy.

The STP is basically a miniature thermocouple (TC) which is thermally biased with respect to the sample and separated from it by a small air gap (Fig. 1). In closed loop operation, the voltage of the TC is stabilized by a feedback system that adjusts the gap such that the tip traces a contour of constant temperature [2], [3]. If the variation in temperature across the sample surface is small compared to the thermal bias, the contour provides a topographic map of the sample. The STP is also useful for a variety of thermography applications, including high resolution photothermal absorption spectroscopy, microelectronics metrology, microflow measurements, and for biological applications like mapping the temperature of a living cell to investigate its metabolic functions [4]–[6]. For several applications of the STP, lateral resolution of  $\approx 1 \mu\text{m}$  is adequate.

There are two scan modes in which the STP can be operated: the DC mode and the dithered mode. In the former, the tip is rastered across the sample while the air gap is controlled to keep the TC signal constant. In the latter, the tip is oscillated perpendicular to the sample, modulating the air gap by about 10%. Dithering the tip can reduce sensitivity of the TC signal to fluctuations in the ambient temperature and also improve the signal-to-noise ratio.

The original STP used a tungsten wire probe with a conical tungsten-nickel tip  $<100$  nm in diameter. The Seebeck coefficient of a tungsten-nickel TC is about  $18 \mu\text{V}/^\circ\text{C}$ . The thermal bias between the tip and the sample was generally provided by heating the sample with an incident laser beam. The best reported spatial resolution was  $\approx 1$  nm vertically, and 30 nm laterally, which was consistent with the probe tip dimensions

[2], [3], [7], [8]. The detection electronics used in this case could resolve  $<1$  mK in a 100 Hz bandwidth.

Separating the effects of temperature and topography in an STP scan is a concern only if both vary simultaneously across a sample surface. In such cases it is possible to separately map the temperature and topography in a single scan if the thermal bias can be pulsed. If the dither frequency is  $f_1$  and the sample is heated at a frequency  $f_2$  which is outside the range of the feedback loop controlling the air gap, then the topographic map can be obtained by monitoring the TC signal at  $f_1$  and the temperature map can be simultaneously obtained by monitoring the signal at the beat frequency  $f_2 - f_1$  [8]. If the thermal bias cannot be pulsed it becomes necessary to monitor the topography by a separate interaction of the tip. For example, a technique has been reported in which a tunneling current established between a metal tip and the sample is used to map topography, while temperature is monitored by the TC formed by the dissimilar conductors of the tip and the sample [9]. Another device combines the functions of an AFM and an STP: thin wires of chromel and alumel microwelded together at the tip of a V-shape form a TC, while a piece of aluminum foil glued to them serves as a reflector for optical readout of the tip deflection [10].

In all the devices discussed above, the temperature measurements were performed by TC's. Scanning temperature measurements have also been performed using an AFM to detect the contact potential between a tip and sample, which is a function of temperature [11]. The advantage of this method is that a TC does not have to be fabricated at the scan tip. However, the temperature-dependent variation of the contact potential between the tip and the sample must be known for all sample materials. Infrared detectors with appropriate focusing optics offer another option for scanning temperature measurements, but the spatial resolution is limited by the radiation wavelength to several microns, and the temperature resolution is typically no better than about 0.1 K [12].

### *Micromachining and Scanning Probe Microscopy*

Research activity aimed at developing lithography-based micromachining techniques for scanning probes is motivated largely by the controllability and reproducibility of these techniques as compared with the more traditional customized shaping and sharpening of thin wires. Additionally, lithography-based processing is better suited for scaling down the device dimensions, for fabricating arrays of devices, and for integrating probes with support circuitry. Smaller probes are better able to resist unwanted vibration and thermal drift. Arrays of probes can be useful in reducing data acquisition times by providing parallel input from several points, as well as enhancing reliability through redundancy. Circuitry integrated onto probe platforms can enhance sensitivity and possibly reduce system costs of scanning microscopes. In addition, microfabrication techniques provide access to a great diversity of materials and tools that can extend the capabilities of scanning probe microscopes.

Previous work on micromachined scanning probes demonstrates the versatile use of various transducing phenomena such

as piezoelectricity, piezoresistance, and capacitance to support AFM and STM applications [13]–[19]. Micromachining technology has not only enhanced the capability and diversity of scanning microscopy tools, but has also triggered the development of other devices based on near-field interactions. Accelerometers, infrared detectors, and pressure sensors based on tunneling current sensing have recently been reported [20]–[24].

In this paper, we describe the design and fabrication of scanning thermal profilers using an IC-compatible lithography-based process. We also describe the thermal characterization of these silicon micromachined thermal profilers (SMTP's), demonstrate their basic functionality, and discuss some theoretically obtained performance limits [25]–[27]. The structure and theory of the SMTP are presented in Section II, the fabrication technology is described in Section III, and experimental results are discussed in Section IV.

## II. STRUCTURE AND THEORETICAL ANALYSIS

A schematic of the basic SMTP design is shown in Fig. 2. The scanning probe overhangs the glass substrate, and is integrated with a suspension which includes flexible support beams and electrostatic comb drives for longitudinal actuation. A thin film TC runs along the probe, with one junction near the protruding metal tip and another near the suspension. Insets in Fig. 2 compare the TC junctions of the SMTP and the original tungsten wire STP. A polysilicon resistive heater located on the lower surface of the suspension provides a convenient option for generating the thermal bias between the tip and the sample. The insulating glass substrate allows the thermal bias to be generated efficiently. As will be discussed later, this basic SMTP design can be modified for higher performance. In this section, thermal issues of importance to the SMTP are examined first, mechanical characteristics of the silicon suspension are briefly discussed next, and the noise limits of the SMTP performance are evaluated last.

### *A. Thermal Issues*

Available thin-film technologies offer a wide choice of materials for the TC. We have selected polysilicon for one side of the TC because it can provide a very high Seebeck coefficient; the other side is Au. A conventional figure of merit for the thermoelectric properties of a material is  $z = S^2/\kappa\rho$ , where  $S$ ,  $\kappa$ , and  $\rho$  denote the Seebeck coefficient, thermal conductivity, and electrical resistivity, respectively. Low values of  $\kappa$  and  $\rho$  are desirable to minimize unwanted heat flow between TC junctions and Johnson noise in the output voltage. However,  $S$  and  $\rho$  are directly related in polysilicon, which leads to a compromise between signal strength and electrical noise. At high doping levels the thermal conductivity due to electrons causes  $z$  to deteriorate in semiconductor TC's even though electrical resistivity drops. The highest  $z$  for polysilicon TC's is at the intermediate doping concentration of  $\approx 10^{19}$  cm $^{-3}$  [28]–[30].  $S$  is higher in n-type polysilicon than in equivalently doped p-type polysilicon, and at intermediate doping levels it lies at 50–100  $\mu$ V/K.

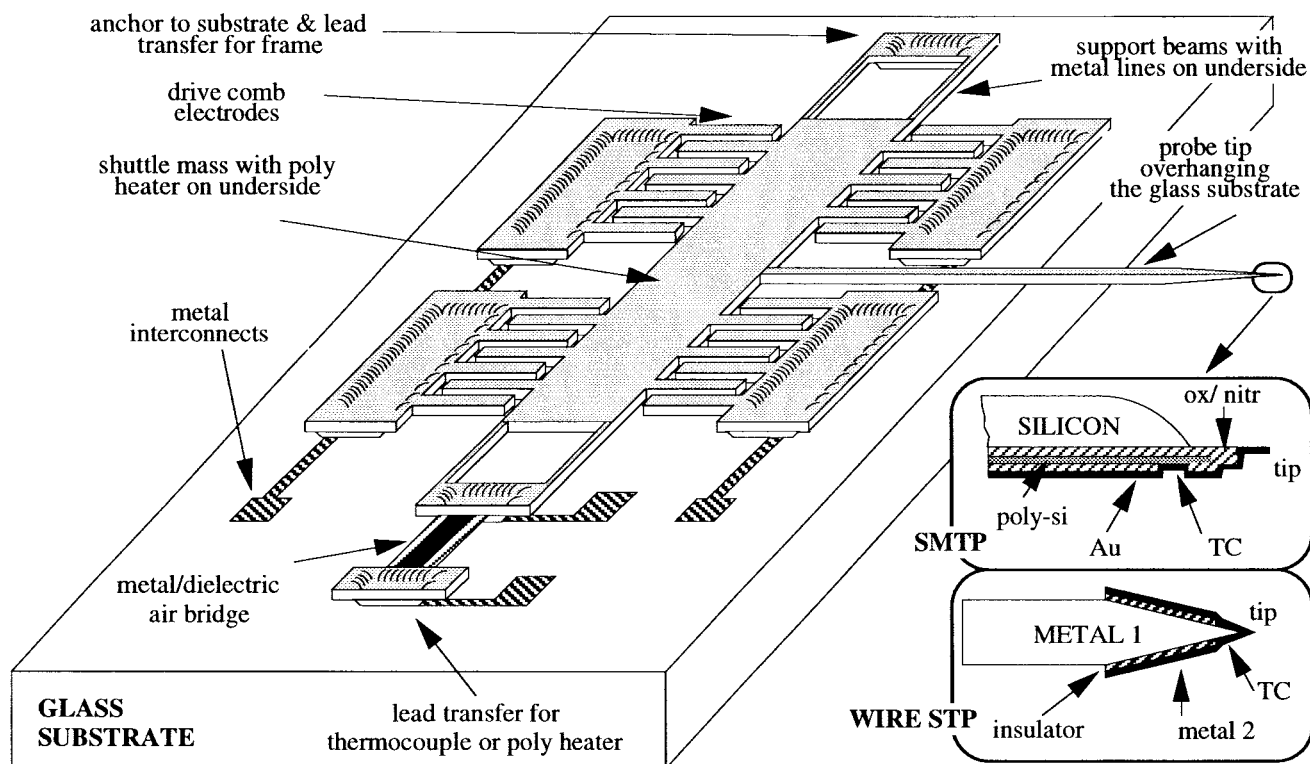


Fig. 2. A schematic identifying the various elements of the SMTP. The insets compare the details of the SMTP tip with the original tungsten wire STP [2].

Heat transfer between the SMTP and the sample is primarily by conduction through the air gap. Natural convection can be neglected because the small dimensions of the probe yield a low Rayleigh number, and forced convection due to scanning motion can similarly be neglected because of a low Reynolds number. Radiation effects are also negligible because the temperature bias maintained between the sample and probe is typically  $\approx 100$  K. In general, the thermal conduction between the tip and the sample is a complex function of the gap size and the tip diameter. The mean free path of nitrogen molecules at atmospheric pressure is about  $872 \text{ \AA}$  at  $373 \text{ K}$ . If the gap is much larger than the mean free path, its thermal resistance can be calculated using the viscous thermal conductivity of the gas, which is about  $3.0 \times 10^{-4} \text{ W/cm K}$  at  $373 \text{ K}$ . The thermal conductance per unit area is the ratio of thermal conductivity to gap size, and for a  $1 \text{ }\mu\text{m}$  gap it is  $3 \text{ W/cm}^2 \text{ K}$ . If the gap is much smaller than the mean free path the thermal conductance per unit area is much larger and independent of the gap size [31], [32].

The simplest approximation of the thermal resistance of the air gap is a cylinder of air with the same cross section as the tip. Fringing effects are absorbed into a correction factor known as the excess flux coefficient,  $\eta'$ , which can be found by numerically solving the equation  $\nabla^2 T = 0$  in the air gap assuming isothermal tip and sample surfaces [33]. When the air gap is much smaller than the tip diameter,  $\eta'$  approaches unity, whereas, when the gap is larger than the tip diameter,  $\eta'$  may exceed 10.

Fig. 3 was obtained by steady state finite element analysis (FEA) of a  $300\text{-}\mu\text{m}$  long,  $40\text{-}\mu\text{m}$  wide,  $10\text{-}\mu\text{m}$  thick silicon probe with a  $10\text{-}\mu\text{m}$  long,  $0.5\text{-}\mu\text{m}$  thick triangular Au tip of  $1$

$\mu\text{m}$  width at its apex, positioned  $1 \text{ }\mu\text{m}$  away from the sample. Exploiting the longitudinal symmetry of the probe only half of it is modeled. It is bounded by adiabatic surfaces laterally, and by isothermal surfaces at  $100$  and  $0 \text{ }^\circ\text{C}$  near the tip and the suspension, respectively. The thermal conductivity of the air is approximated by its value at the viscous limit for simplicity. It can be seen that the temperature of the probe remains almost constant for most of its length. The temperature of the metal tip is just below  $1 \text{ }^\circ\text{C}$ , indicating that the temperature drop across the TC is about 1% of the temperature bias. The contours also show evidence of substantial fringing effects. Fringing effectively increases the coupling between the tip and the sample, enhancing temperature sensitivity of the SMTP at the cost of lateral spatial resolution. Repeating the FEA for a gap of  $0.1$  and  $0.09 \text{ }\mu\text{m}$ , it is seen that the temperature change in the middle of the metal tip is  $\approx 3 \text{ K}/\mu\text{m}$ . If the  $S = 100 \text{ }\mu\text{V/K}$  and the detecting electronics can resolve  $1 \text{ }\mu\text{V}$ , this implies that, neglecting noise, the spatial resolution perpendicular to the sample is  $3.33 \text{ nm}$  at  $100 \text{ nm}$  separation. Since the region of the sample surface that interacts thermally with the device increases not only with the tip diameter but also with the air gap, the lateral spatial resolution of the scan is limited by the larger of these two dimensions. As the gap increases, the interaction diminishes in a much more gradual manner than it does for AFM's and STM's. Scanning thermal microscopy, therefore, permits a compromise between lateral resolution and operating gap that is not afforded by these other techniques.

For most scans performed with scanning thermal profilers the thermal resistance of the air gap is much larger than the thermal resistance between points within the sample, or between the sample and its support. The SMTP tip, therefore,

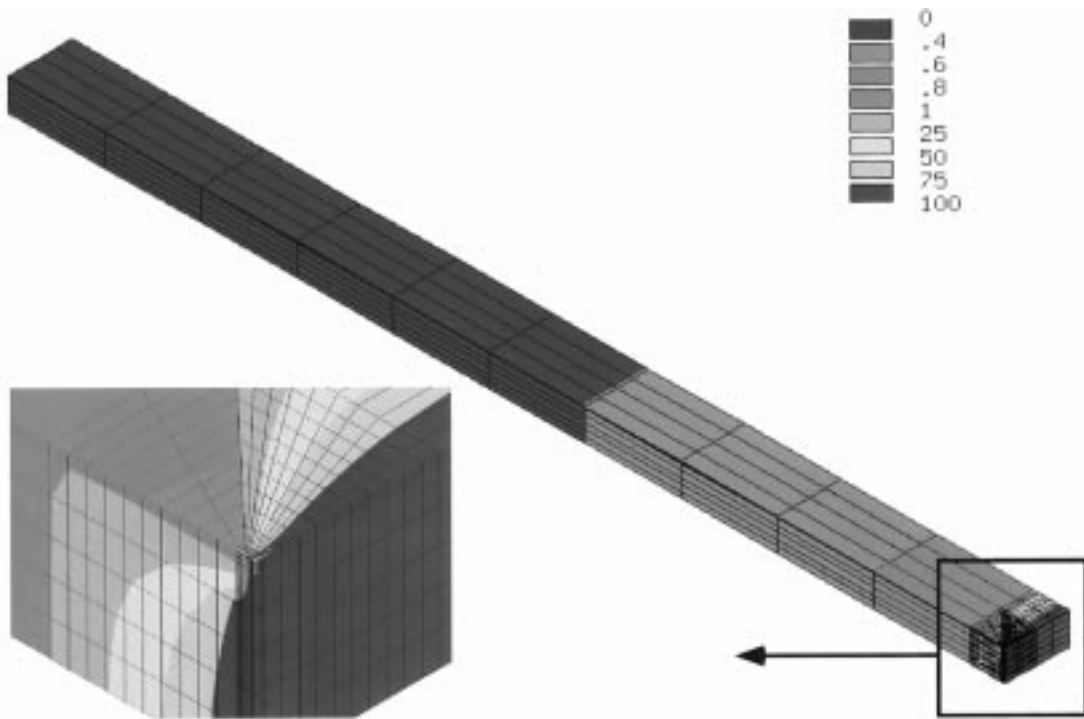


Fig. 3. Steady-state temperature distribution along the probe shank of design A obtained by FEM. One longitudinal half of the volume is shown, and the viewing angle is from below the shank and across the plane of symmetry. The tip-sample region is magnified in the inset, showing the lateral spread of the interaction.

should not significantly affect the temperature of the sample. It is possible, however, that the parasitic heat loss mechanisms of the sample, including convection, etc., are affected to some extent by the presence of the assembly and support structure of the SMTP. These are longer range interactions, and it is reasonable to expect that they will not modulate the signal from a scanned probe, although they might affect its offset.

It is instructive to examine a simple one-dimensional electrical equivalent model for the conductive heat transfer as illustrated in Fig. 4. Once again, the sample and the base of the probe are assumed to be at fixed temperatures  $T_o$  and  $T_{sh}$ , respectively. The thermal impedance of the probe shank ( $Z_{TC}$ ), and the thermal resistance of the air gap ( $R_g$ ) form a divider. The voltage read out from the TC is a measure of the temperature drop across  $Z_{TC}$ . Under steady state conditions the variation of this voltage with gap size  $x$  is given by:

$$\frac{dV_{TC}}{dx} = \frac{-\eta' S Z_{TC} T_B}{A_t \kappa (Z_{TC} + R_g)^2} \text{ assuming that } R_g = \frac{\eta' x}{A_t \kappa} \quad (1)$$

where  $A_t$  is the area of the tip and  $T_B = (T_o - T_{sh})$  is the thermal bias. In addition to the intuitively obvious dependence on  $S$  and  $T_B$ , (1) shows that the vertical resolution will drop as  $Z_{TC}$  approaches either zero or infinity. These are, respectively, the trivial cases in which the TC probe either sustains no temperature bias or allows no heat flow. The optimal value (from this perspective) of  $Z_{TC} = R_g$  is difficult to achieve with large air gaps because the thermal conductivity of the probe materials is four orders of magnitude higher than that of air. Extending this analysis to the dithered mode of operation, if  $Z_{TC}$  is modeled by a resistor and capacitor in parallel, it

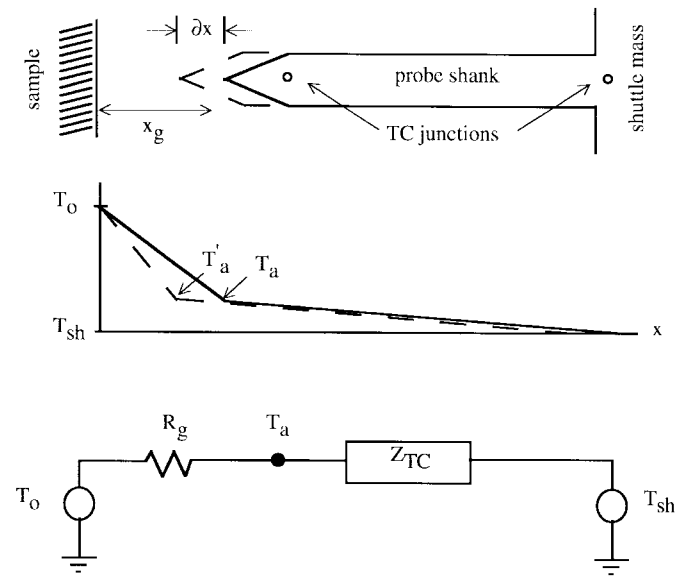


Fig. 4. A one-dimensional model for the conductive heat transfer between the sample and the SMTP.

becomes evident that the thermal capacitance of the probe shank must be minimized to improve its temporal response.

In addition to the SMTP design illustrated in Fig. 2, this paper describes two designs with increased thermal resistance and reduced thermal capacitance along the probe shank. The basic silicon shank SMTP is labeled design A. In design B, the silicon shank is split longitudinally to form the rim for a dielectric diaphragm which supports the TC. Design C also has a dielectric diaphragm, but has a 7-junction thermopile

instead of a single thermocouple for higher sensitivity. All three designs for the SMTP have been implemented and tested, and their performances are compared in Section IV.

*B. Mechanical Characteristics*

As shown in Fig. 2, the SMTP probe is supported by a bridge-like mechanical frame which can be actuated by comb drives [34]–[36]. Comb drives circumvent problems of parallel plate capacitive actuators such as nonlinear force-displacement relationships and strong squeeze-film damping, and are particularly favorable for long-throw actuators. The motion is driven by applying a voltage across one set of combs, and sensed by monitoring the output current from another set of combs across which is a fixed voltage bias.

In the dithered mode of operation, the SMTP may be driven at resonance if large amplitude motion is desired, or at a lower frequency if small amplitude motion and insensitivity of amplitude to driving frequency are preferred. It should be noted, however, that if there are resonant modes in the system at lower frequencies than the fundamental lateral mode, they could possibly interfere with the device operation. For example, a torsional mode might cause out-of-plane motion of the probe tip and lead to a loss in spatial resolution.

In the SMTP thin-film gold leads for the TC and the integrated resistive heater run along the flexural beams. All four beams have identical geometry and composition, so the structure is symmetric. The gold is insulated from the silicon by oxide and nitride films with thickness ratioed to nullify residual stress. In addition to having low composite stress these films are also very thin, so the mechanical behavior of the composite structure is very close to that of the Si frame alone. Details of the SMTP suspensions are discussed in [35].

*C. Noise Limitations Inherent to SMTP Performance*

Noise within the SMTP can be electrical, mechanical, or thermal in origin. The electrical noise arises from the resistance of the polysilicon lead in the TC:

$$N_e = \frac{\langle V_N^2 \rangle}{B} = 4k_b T R_{TC} \left( \frac{V^2}{\text{Hz}} \right) \quad (2)$$

where  $B$ ,  $k_b$ ,  $T$ , and  $R_{TC}$  are the measurement bandwidth, Boltzmann’s constant, the average temperature, and the electrical resistance of the polysilicon line, respectively. For a 50 square long polysilicon line with a sheet resistance of 100  $\Omega/\text{sq.}$ ,  $N_e = 8.9 \times 10^{-17} \text{ V}^2/\text{Hz}$  at 323 K. Flicker noise in the TC contacts can be ignored because the TC is usually connected to a buffer with high input impedance, and the current flowing through these contacts is negligible.

At atmospheric pressure, noise in the mechanical regime is due to random impact from molecules in the fluid around the resonator. The spectral density of the mechanical noise at frequencies well below resonance may then be stated as:

$$N_m = \frac{\langle Y_N^2 \rangle}{B} = \frac{4k_b T c}{k^2} = 4k_b T \left[ \frac{1}{QM(2\pi f_o)^3} \right] \left( \frac{m^2}{\text{Hz}} \right) \quad (3)$$

where  $c$ ,  $k$ ,  $Q$ ,  $M$ , and  $f_o$  are the damping coefficient, the spring constant, the mechanical quality factor, the mass, and

the resonant frequency, respectively. Typical values of  $M$ ,  $f_o$ , and  $Q$  for the SMTP are  $4 \times 10^{-10} \text{ Kg}$ , 30 KHz, and 100. Thus, the rms noise displacement is  $\langle Y_N \rangle \approx 8.16 \times 10^{-15} \text{ m}/\sqrt{\text{Hz}}$ , which is clearly negligible. If this was not negligible, its net contribution would be evaluated by calculating its effect upon the air gap, the consequent effect upon the tip temperature, and from that the effect on the TC signal.

There is Johnson noise associated with the transfer of heat between the device and its surroundings that can be written as [37]:

$$N_t = \frac{\langle \Delta T_N^2 \rangle}{B} = \frac{4k_b T^2 R_t}{1 + (2\pi f R_t C_t)^2} \left( \frac{K^2}{\text{Hz}} \right) \quad (4)$$

which is inversely related to the dither frequency. For a  $300 \mu\text{m} \times 40 \mu\text{m} \times 10 \mu\text{m}$  Si shank,  $C_t$ , the thermal capacitance of the device, is  $2.2 \times 10^{-7} \text{ J/K}$ . For the worst-case noise at low frequencies,  $R_t$ , the thermal resistance between the device and the environment, can be approximated by the thermal resistance between the tip and the sample, so  $R_t = R_g = 3.85 \times 10^6 \text{ K/W}$ , assuming viscous conduction across a  $0.1 \mu\text{m}$  long gap with a cross-sectional area of  $1 \mu\text{m}^2$ . (In reality,  $R_t$  can be much smaller.) The mean square voltage noise in the TC due to this effect is found by evaluating (4) at  $f = 0$ :

$$\langle V_{Nt}^2 \rangle = \langle \Delta T_N^2 \rangle S^2 = 4k_b T^2 R_g B S^2 (V^2). \quad (5)$$

At 323 K, with  $S = 100 \mu\text{V/K}$ , it is  $2.22 \times 10^{-19} \text{ V}^2/\text{Hz}$ —about 2 orders of magnitude less than the electrical noise obtained from (2). Under the assumed conditions, therefore, the Johnson noise associated with heat transfer can be ignored.

These calculations indicate that the inherent noise performance of the device is limited by the resistance of the polysilicon lead of the TC. For  $R_{TC} = 5 \text{ K}\Omega$  at 323 K, the rms noise is about  $9.4 \text{ nV}/\sqrt{\text{Hz}}$ . The noise equivalent temperature difference (NETD) for the SMTP can be written as:

$$\text{NETD} = \frac{\sqrt{4k_b T B R_{TC}}}{S} (K). \quad (6)$$

In a 100 Hz bandwidth the NETD is 0.94 mK for the parameters described above. One way to improve this is to reduce the electrical resistance of the polysilicon line by making it wider and thicker. Since the thermal conduction between the two TC junctions is dominated by the  $p^+$  Si probe shank, these changes will not affect the temperature distribution, and will make it possible to reduce the NETD without sacrificing sensitivity. The polysilicon resistance may also be reduced by increasing its doping, but this is not a good option since it will diminish  $S$ , as mentioned previously.

In addition to the noise inherent to the micromachined device, the system has noise from the external electronics, the scanning equipment, and the mechanical fixture. As will be shown Section IV, these sources of noise can easily dominate and limit performance.

III. FABRICATION

The approach selected for fabricating the SMTP is a bulk silicon micromachining technique known as the dissolved wafer

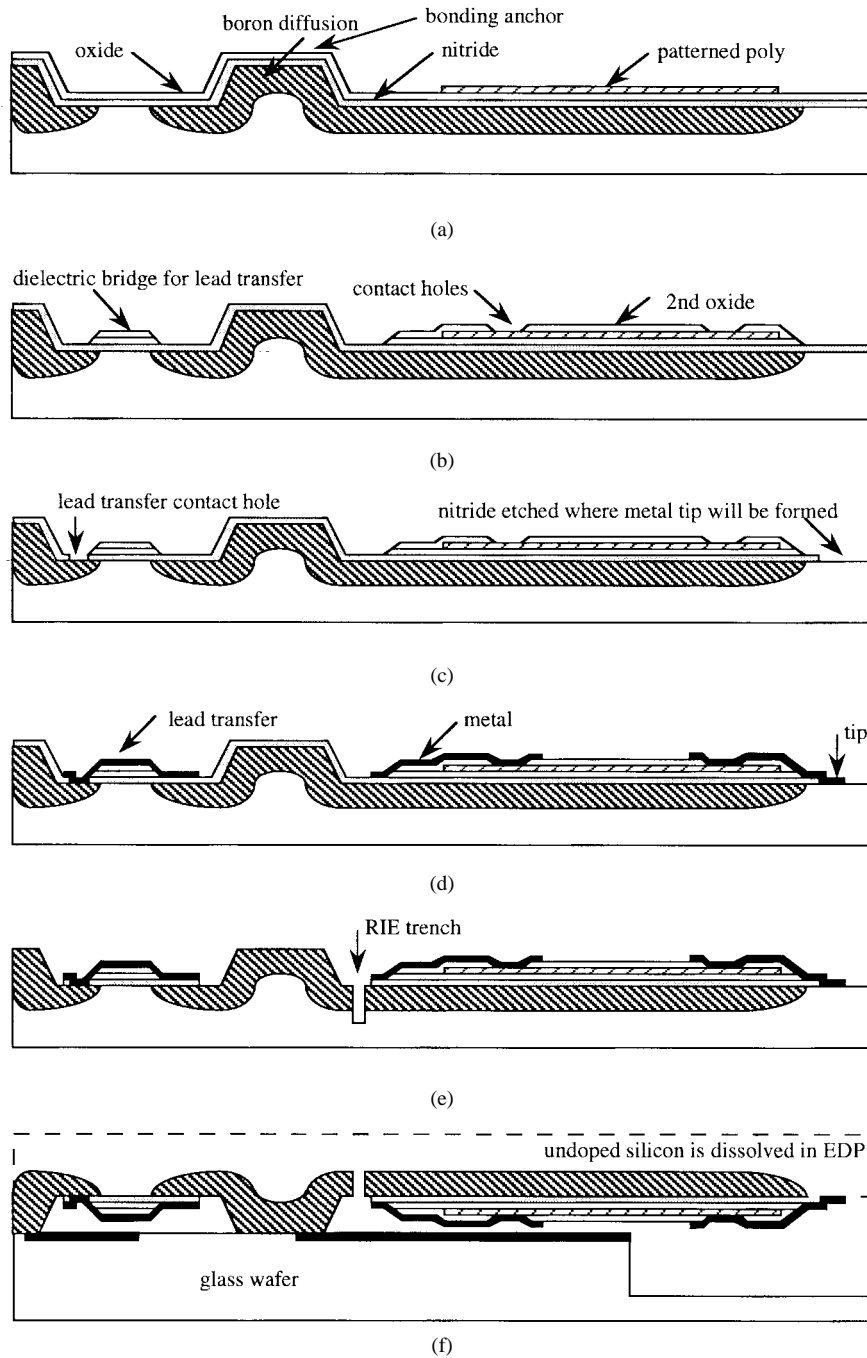


Fig. 5. The 8-mask IC-compatible fabrication sequence for SMTP's. Details are described in the text.

process (DWP). Boron diffusion provides an impurity-based etch stop for silicon microstructures while the remainder of the wafer is etched away [35], [38]–[40]. The DWP is particularly suitable for SMTP fabrication: it facilitates structures with thickness-to-width aspect ratios in excess of 10:1, benefiting the capacitive comb drive as well as mechanical robustness; overhanging probes can be fabricated with no extra effort; low expansion mismatch between structural and substrate materials yields relatively small temperature coefficients of performance; boron doped silicon has low residual stress that is tensile and symmetrically distributed across the depth of the structure, which prevents buckling and out-of-plane deformation [41], [42]. The DWP permits the fabrication of microstructures with

on-chip circuitry [40], [43], as do some other micromachining techniques. Although not exploited for the research described in this paper, this feature provides an avenue for continued improvement of scanning tips. The DWP has been used for a variety of devices in the past, including accelerometers [24], comb resonators [35], stacked mechanical linkages [38], neural probes [43], tactile imagers [44], flow sensors [45], gyroscopes [46], [47], valves [48], and ink-jet nozzles [49].

The same 8-mask fabrication sequence (Fig. 5) can be used for all three SMTP designs described previously. A (100) oriented standard silicon wafer is recessed by 3–5 μm, forming mesas to anchor the mechanical frame and assist in the transfer of electrical leads to the glass substrate. Boron is diffused into

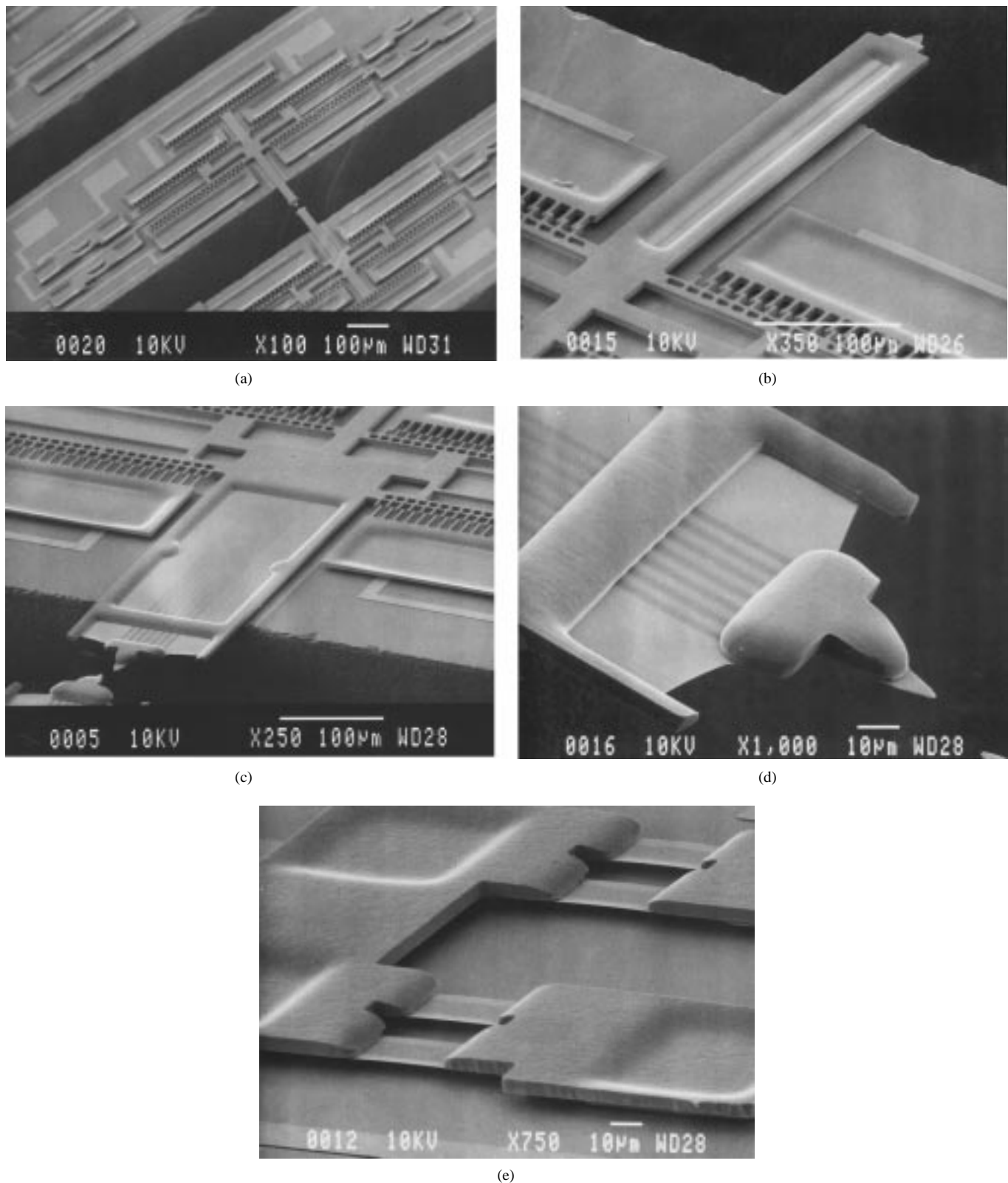


Fig. 6. Scanning electron micrographs showing various views of SMTF devices with (a) a silicon shank, (b) a dielectric shank, (c) a 7 junction thermopile on a dielectric shank, (d) a close-up of the multi-junction tip, and (e) shows a close-up view of the lead transfer over a dielectric bridge.

the structural regions where the probe and its comb-driven suspension will be defined. Field regions as well as the parts of probe shanks in which dielectric diaphragms will be formed are masked from the diffusion by a thick layer of oxide. The diffusion depth determines the height of the microstructures:

regions doped more than  $\approx 5 \times 10^{19} \text{ cm}^{-3}$  will be retained after the silicon wafer dissolution. The diffusion is followed by low pressure CVD of nitride, oxide, and polysilicon. The polysilicon is doped with phosphorus, annealed, and patterned to form the on-board heater and one side of the TC [Fig. 5(a)].

The oxide beneath it serves as an etch stop for this patterning step, and also provides electrical and thermal isolation between the TC and the mechanical frame. The nitride provides stress compensation. Next, the polysilicon is insulated from above using thermal and LPCVD oxides. A wet etch opens contact holes to it and simultaneously strips the field oxide [Fig. 5(b)]. Oxide is retained in certain regions to form dielectric bridges that support metal lead transfers to the isolated bond islands. The exposed nitride is dry etched for contacts to the isolated bond anchors [Fig. 5(c)], and then gold is deposited and patterned to form the second side of the TC, the scanning tip, and the interconnect [Fig. 5(d)]. A Ni thin film is then patterned to mask a reactive ion etch (RIE) that traverses the entire thickness of the  $p^+$  Si, defining the fine features of the mechanical frame [Fig. 5(e)]. Finally, the Ni is stripped and the nitride removed from the anchors in preparation for electrostatic bonding.

The glass substrate wafer is inlaid with Au interconnect, grooved for overhanging features and die separation, and then electrostatically bonded face-to-face with the Si wafer [35]. Leads are transferred automatically where metal on the glass overlaps the silicon bonding anchors. The sample is then immersed in EDP to dissolve the undoped silicon, releasing the finished devices [Fig. 5(f)]. Overhanging features are formed wherever boron diffused silicon extends above grooves in the glass substrate.

Fig. 6(a)–(d) show scanning electron micrographs of the three different SMTP designs. Fig. 6(a) shows a complete silicon shank device, with three banks of combs on one side of the shuttle mass and two banks on the other side. The suspension beams are 4  $\mu\text{m}$  wide, and 200–400  $\mu\text{m}$  long; the probes are  $\approx 300 \mu\text{m}$  long, and extend over grooves in the glass substrate, facing each other. Fig. 6(b) shows a probe with the TC isolated on a dielectric diaphragm. The metal and polysilicon lines of the TC are coincident, separated by an oxide layer. The inner edges of the  $p^+$  silicon rim that surrounds the diaphragm show the characteristic curvature of a diffusion profile, whereas the outer edges, which were defined by RIE, are vertical. Fig. 6(c) and (d) show a probe with a 7 junction thermopile suspended on a dielectric diaphragm. A  $p^+$  silicon rib runs across the width of the probe to enhance mechanical support. A small silicon mass is suspended near the tip to provide a thermal short across the thermopile junctions located there; it is electrically connected to the center junction only. All three devices shown in Fig. 6(a)–(d) are 8  $\mu\text{m}$  thick. Fig. 6(e) shows the lead transfer accomplished with a dielectric bridge which is structurally quite similar to the diaphragms that isolate the TC's. The metal line that runs along the bridge, visible in silhouette in the figure, makes electrical contact with one anchor, transferring the signal through it to the glass interconnect. It is isolated from the other anchor by dielectrics. The bridge provides low capacitance and low resistance lead transfer for electrical elements integrated with the actuator.

The diameter of the metal scanning tip of the SMTP is limited by the resolution of the lithography tool. Since the tip is patterned at the bottom of a trench formed when the anchors are defined, the limited depth-of-focus of the aligner can cause the tip diameter to be as large as 1  $\mu\text{m}$  [Fig. 6(d)]. One way

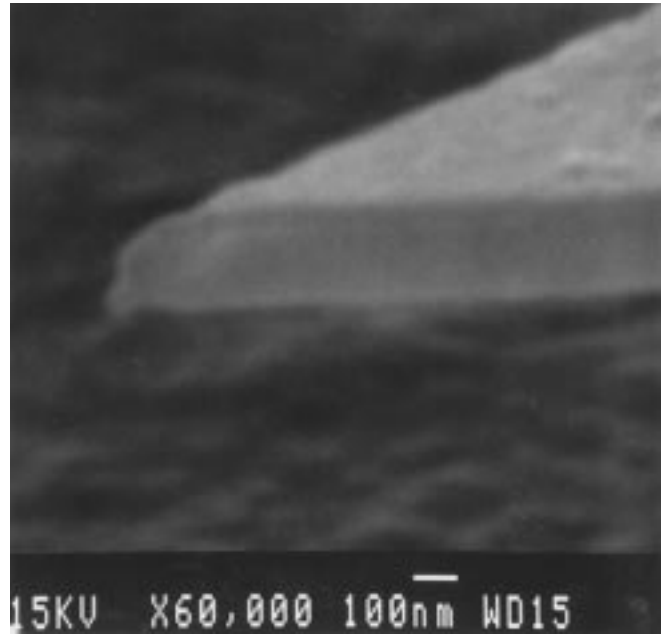


Fig. 7. A metal tip with 1000  $\text{\AA}$  diameter and 2000  $\text{\AA}$  thickness formed by two masking steps.

to circumvent this problem is to use separate masks to define the two sides of the tip, so that its sharpness is not limited by the lithography. Fig. 7 shows an Al tip fabricated to illustrate this idea: its lithographically defined diameter is much smaller than its 2000  $\text{\AA}$  thickness.

In summary, the fabrication process developed for the SMTP's permits the incorporation of electrical elements such as thermocouples and heaters onto comb driven frames, the suspension of these elements on dielectric diaphragms, and the transfer of multiple electrically isolated leads from the device onto interconnect patterned on the glass substrate.

#### IV. MEASUREMENT AND CHARACTERIZATION

The mechanical characterization of DWP comb drive suspensions is detailed in [35]. The fundamental mode resonant frequencies that can be achieved for dimensions typical of the SMTP are  $< 100 \text{ KHz}$ ;  $Q$  in air is 50–150; peak–peak motion achievable with a 25 V square wave is  $< 20 \mu\text{m}$ ; Young's Modulus and residual stress are  $\approx 175 \text{ GPa}$  and 15–30 MPa, respectively.

For thermal characterization the SMTP tip is brought into contact with a large heat sink, such as a micromanipulator probe, forcing one TC junction to room temperature. The other junction, which is located on the shuttle mass, is heated by applying a voltage (or current) ramp across the polysilicon resistor near it. The plot of the TC voltage versus the heater input power is linear, demonstrating that the heat transfer is primarily conductive (Fig. 8). The slope of this plot, which is typically several hundred millivolts per watt of input power to the heater for single TC devices (designs A and B), provides a useful measure of their thermal characteristics. When the same measurement is repeated with the heat sink removed from the SMTP tip, the slope of the response is proportional to the parasitic heat loss along the probe. The difference between

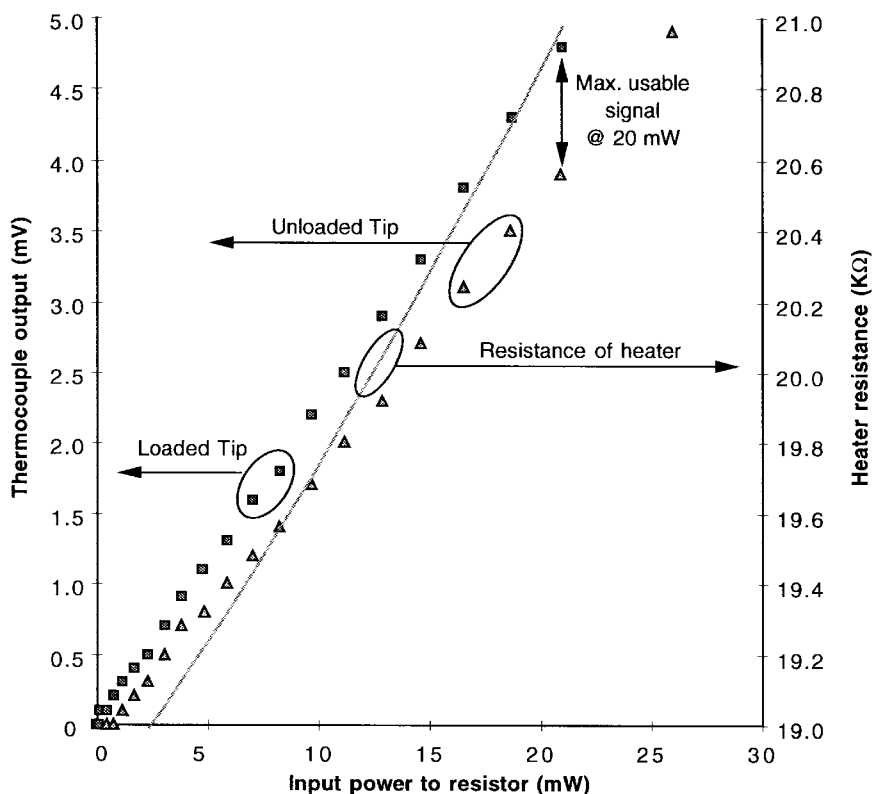


Fig. 8. Thermal response curves for an SMTP with a solid silicon shank with and without the tip loaded by contact to a large heat sink at room temperature. Using the TCR of the heater (900 ppm/K), and the resistance curve shown above, the TC output can be expressed as a function of temperature, yielding the Seebeck coefficient of the TC. Typical values obtained ranged from 40  $\mu\text{V/K}$  (shown above) to 80  $\mu\text{V/K}$ .

TABLE I  
COMPARISON OF THERMAL CHARACTERISTICS  
OF THREE SMTP DESIGNS.  $S = 80 \mu\text{V/K}$

| Shank type               | Si-1 TC (A) | Diel.-1 TC (B) | Diel.-7 TC (C) | Units       |
|--------------------------|-------------|----------------|----------------|-------------|
| Loaded (L)               | 579         | 741            | 4563           | mV/W        |
| Unloaded (U)             | 531         | 606            | 3739           | mV/W        |
| <b>Max. signal (L-U)</b> | <b>48</b>   | <b>135</b>     | <b>824</b>     | <b>mV/W</b> |

the two measurements at each value of heater input power provides the maximum useful signal available from the TC. Values for this vary from a few tens to a few hundreds of mV/W depending on the nature of the shank and the polysilicon used. Table I lists the responses of three SMTP's found near each other on a wafer. The design change from a Si shank (design A) to a dielectric shank (design B) alone offers an improvement of almost 3 $\times$ , and using the 7-junction thermopile (design C) offers a further improvement of more than 6 $\times$ .

The temperature coefficient of resistance (TCR) of the on-board heaters was measured in the temperature range of 50–150°C and found to be 900 ppm/K. Knowing this, the temperature of the heater can be determined from its  $I$ - $V$  curve. For tests in which the tip is held at room temperature by a large heat sink, the TC output voltage can, therefore, be plotted as a function of temperature to find the Seebeck coefficient. Typical values obtained were 40–80  $\mu\text{V/K}$ . Additionally, the ratio of the heater temperature to its input power is the net thermal resistance to the ambient—an estimate of the thermal isolation achieved by the device. Typical values

obtained were 5000–10 000 K/W with the tip held at room temperature. These numbers may vary with the mounting and placement of the device.

One-dimensional scans were obtained both with and without dither motion to demonstrate functionality of the fabricated devices. The sample used was an 80  $\mu\text{m}$  wide, 15  $\mu\text{m}$  thick silicon probe designed for neural prosthesis applications, supporting a polysilicon resistor insulated from above by 5000 Å of oxide. The polysilicon lines were  $\approx 7500$  Å thick, 10  $\mu\text{m}$  wide, and 20  $\mu\text{m}$  apart. The thermal bias was generated by passing a current through the resistor in the sample instead of the SMTP. The sample was mounted on a piezoelectric bimorph, which provided the raster motion. The air gap between the sample and the scanning tip was adjusted manually. A DC scan obtained using a silicon shank SMTP (design A) is shown in Fig. 9(a). A low noise amplifier and an HP 4145B DC parametric analyzer were used to monitor the TC voltage. Temperature resolution was limited to  $\approx 20$  mK by noise in the test set-up; spatial resolution was limited by the tip dimension and air gap to  $\approx 1 \mu\text{m}$ . A dithered scan [Fig. 9(b)] was obtained by electrostatic actuation of the combs. The signal was detected using a lock-in amplifier. Unwanted mechanical vibrations in the set-up and problems with the scanning motion are evident in the measured data. These problems, however, can be largely eliminated by using more sophisticated scanning apparatus that is available commercially.

Fig. 10 shows the SMTP response as a heated sample (similar to the one used in the scans) approaches it from a distance. The TC signal increases rapidly with the current

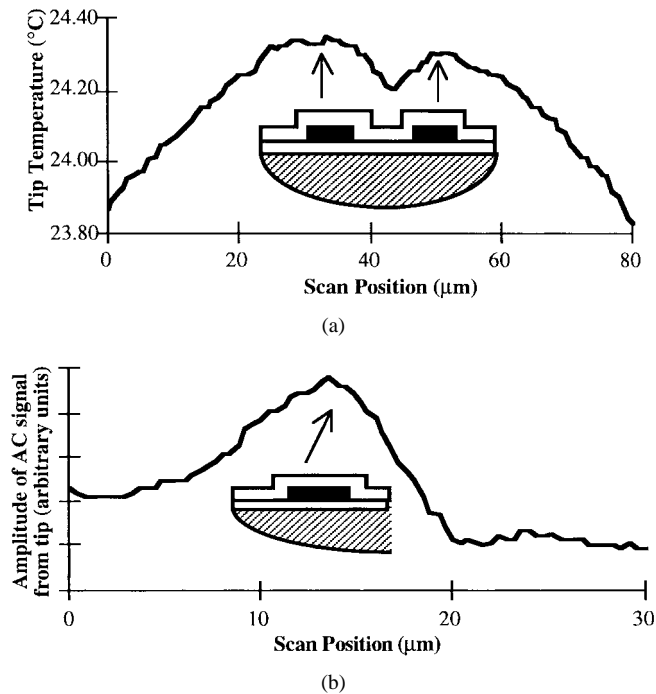


Fig. 9. (a) A nondithered scan of two polysilicon lines which are segments of a  $32\text{ K}\Omega$  resistor carrying  $500\ \mu\text{A}$ . (b) A dithered scan of a single line of a similar resistor carrying  $1\ \text{mA}$ .  $S = 40\ \mu\text{V/K}$ .

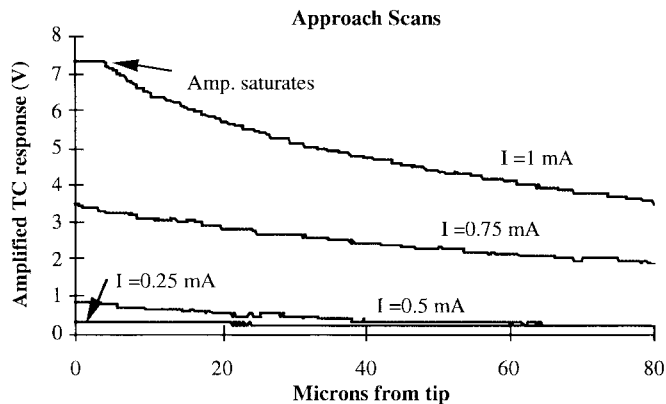


Fig. 10. The response of an Si shank SMTP as the current-heated test sample approaches it.  $S = 80\ \mu\text{V/K}$ .

supplied to the  $29\text{ K}\Omega$  resistor integrated with the sample. This is expected since the temperature is proportional to the power supplied to the resistor.

## V. CONCLUSION

Spatial resolution of an SMTP depends on the Seebeck coefficient of the TC, the thermal impedance of the probe shank, as well as on operating conditions such as temperature bias, air gap, and the sensitivity of the interface electronics. Operationally, there are significant benefits to spatial and temperature resolution, signal strength, and response speed if the tip is operated close to the sample—perhaps within the mean free path of a gas molecule at atmospheric pressure. However, meaningful scans can also be obtained at much larger gaps than afforded by tunneling and force microscopy.

The tip diameter can be reduced to  $<100\ \text{nm}$ , at which point it is limited by its thickness of the metal layer. However, even with a  $1\ \mu\text{m}$  wide tip and a  $0.1\ \mu\text{m}$  air gap, FEA results indicate that it is reasonable to expect perpendicular spatial resolution to be in the range of  $3.33\ \text{nm}$  for design A. Polysilicon-gold TC's fabricated in this effort have a Seebeck coefficient of  $40\text{--}80\ \mu\text{V/K}$ . The temperature resolution of the tip is limited by Johnson noise in the polysilicon lead of the TC to a calculated value of about  $0.1\ \text{mK}/\sqrt{\text{Hz}}$ . The maximum usable signal obtained with design A is  $48\ \text{mV/W}$  of input power to the integrated heater. Isolating the TC on a dielectric diaphragm along the probe (design B) leads to a  $3\times$  improvement in the response. Using a 7-junction thermopile (design C) instead of a single TC leads to an additional  $6\times$  improvement, resulting in a response of  $824\ \text{mV/W}$ . The overall thermal impedance from the heater to the ambient is  $5000\text{--}10\,000\ \text{K/W}$  with the SMTP tip held at room temperature.

The electrostatic comb-driven suspensions can be designed over a wide range of stiffness, with fundamental mode mechanical resonance frequencies  $<100\ \text{kHz}$  for the device sizes considered. They can be driven electrostatically with signals  $<25\ \text{V}$ , and typically achieve a mechanical quality factor  $>100$  at atmospheric pressure. In general, the electrical, mechanical, and thermal characteristics of SMTP's can be customized to suit particular needs.

The SMTP fabrication technique is based on the bulk silicon dissolved wafer process and requires eight masks. The suspension of the TC on a dielectric diaphragm and the overhang of the probe are accomplished without any extra masking steps. Leads are batch-transferred between the electromechanical frame, electrical components like TC's and heaters that may be built upon it, and interconnect patterned on the glass substrate, with the help of metal air bridges that are reinforced by dielectric layers. The integration of sensing and actuating functions in the SMTP and the use of lithography-based batch fabrication methods are representative of emerging trends in micro-scale transducers.

## ACKNOWLEDGMENT

The authors gratefully acknowledge valuable discussions with Prof. B. Orr, and the assistance of the University of Michigan Solid-State Electronics Laboratory staff.

## REFERENCES

- [1] H. K. Wickramasinghe, "Some history and technology of scanning microscopy," *SPIE Scan. Microsc. Technol. Applicat.*, vol. 897, pp. 2–6, 1988.
- [2] C. C. Williams and H. K. Wickramasinghe, "Scanning thermal profiler," *Appl. Phys. Lett.*, vol. 49, no. 23, pp. 1587–1589, Dec. 1986.
- [3] ———, "High resolution thermal microscopy," in *IEEE Ultrasonics Symp.*, 1986, pp. 393–397.
- [4] H. K. Wickramasinghe, "Scanned-probe microscopes," *Scientific American*, pp. 98–105, Oct. 1989.
- [5] M. Stopka, L. Hadjiiski, E. Oesterschulze, and R. Kassing, "Surface investigations by scanning thermal microscopy," *J. Vac. Sci. Technol. B*, vol. 13, no. 6, pp. 2153–2156, Nov./Dec. 1995.
- [6] E. Oesterschulze, M. Stopka, L. Ackermann, W. Scholz, and S. Werner, "Thermal imaging of thin films by scanning thermal microscope," *J. Vac. Sci. Technol. B*, vol. 14, no. 2, pp. 832–837, Mar./Apr. 1996.

- [7] Y. Martin, C. C. Williams, and H. K. Wickramasinghe, "Tip-techniques for microcharacterization of materials," *Scan. Microsc.*, vol. 2, no. 1, pp. 3–8, 1988.
- [8] C. C. Williams and H. K. Wickramasinghe, "Thermal and photothermal imaging on a sub-100 nanometer scale," *SPIE Scan. Microsc. Technol. Applicat.*, vol. 897, pp. 129–134, 1988.
- [9] J. M. R. Weaver, L. M. Walpita, and H. K. Wickramasinghe, "Optical absorption microscopy and spectroscopy with nanometer resolution," *Nature*, vol. 342, pp. 783–785, Dec. 14, 1989.
- [10] A. Majumdar, J. P. Carrejo, and J. Lai, "Thermal imaging using the atomic force microscope," *Appl. Phys. Lett.*, vol. 62, no. 20, pp. 2501–2503, May 17, 1993.
- [11] M. Nonnemacher and H. K. Wickramasinghe, "Scanning probe microscopy of thermal conductivity and subsurface properties," *Appl. Phys. Lett.*, vol. 61, no. 2, pp. 168–170, July 13, 1992.
- [12] B. Linnander, "When it's too hot to touch use infrared thermography," *Circ. Devices*, pp. 35–37, July 1993.
- [13] S. Akamine, T. R. Albrecht, M. J. Zdeblick, and C. F. Quate, "A planar process for microfabrication of a scanning tunneling microscope," *Sens. Actuators, (Transducers '89)*, vols. A21–A23, pp. 964–970, 1990.
- [14] T. Itoh and T. Suga, "Development of a force sensor for atomic force microscopy using piezoelectric thin films," *Nanotechnology*, vol. 4, pp. 218–224, 1993.
- [15] J. Brugger, R. A. Buser, and N. F. de Rooij, "Micromachined atomic force microprobe with integrated capacitive read-out," *J. Micromech. Microeng.*, vol. 2, pp. 218–220, 1992.
- [16] L. C. Kong, B. G. Orr, and K. D. Wise, "Integrated electrostatically resonant scan tip for an atomic force microscope," *J. Vac. Sci. Technol.*, vol. 11, no. 3, pp. 634–641, May/June 1993.
- [17] M. Tortonese, H. Yamada, R. C. Barrett, and C. F. Quate, "Atomic force microscopy using a piezoresistive cantilever," in *Proc. Int. Conf. on Solid-State Sensors and Actuators (Transducers '91)*, 1991, pp. 448–451.
- [18] M. I. Lutwyche and Y. Wada, "Observation of a vacuum tunnel gap in a transmission electron microscope using a micromechanical tunneling microscope," *Appl. Phys. Lett.*, vol. 66, no. 21, pp. 2807–2809, May 22, 1995.
- [19] Y. Xu, N. C. MacDonald, and S. A. Miller, "Integrated micro-scanning tunneling microscope," *Appl. Phys. Lett.*, vol. 67, no. 16, pp. 2305–2307, Oct. 16, 1995.
- [20] T. W. Kenny, W. J. Kaiser, S. B. Waltman, and J. K. Reynolds, "Novel infrared sensor based on a tunneling displacement transducer," *Appl. Phys. Lett.*, vol. 59, pp. 1820–1822, 1991.
- [21] T. W. Kenny, W. J. Kaiser, J. A. Podosek, H. K. Rockstad, J. K. Reynolds, and E. C. Vote, "Micromachined tunneling displacement transducers for physical sensors," *J. Vac. Sci. Technol.*, vol. A-11, no. 4, pp. 797–802, July/Aug. 1993.
- [22] H. K. Rockstad, T. W. Kenny, J. K. Reynolds, W. J. Kaiser, and T. B. Gabrielson, "A miniature high-sensitivity accelerometer based on electron tunneling transducers," *Sens. Actuators A*, vol. 43, pp. 107–114, 1994.
- [23] C. Yeh and K. Najafi, "Bulk silicon tunneling-based pressure sensors," *Tech. Dig. Solid-State Sensor and Actuator Workshop*, Hilton Head, SC, 1994.
- [24] ———, "A low-voltage bulk-silicon tunneling-based microaccelerometer," in *Dig. Int. Electron Devices Meeting*, Washington, DC, Dec. 1995, pp. 593–596.
- [25] Y. Gianchandani and K. Najafi, "Silicon micromachined thermal profilers," in *Digest, Int. Electron Devices Meet.*, Washington, DC, Dec. 1993, pp. 191–194.
- [26] ———, "Bulk silicon micromachining for the scanning thermal profiler and other applications," in *SPIE Symp. Integrated Optics and Microstructures*, San Diego, July 1994.
- [27] Y. B. Gianchandani, Ph.D. thesis and University of Michigan Solid-State Electronics Laboratory Tech. Rep. no. 240, *A Bulk Silicon Microelectromechanical System for Scanning Thermal Profilometry*, Oct. 1994.
- [28] A. W. van Herwaarden and P. M. Sarro, "Thermal sensors based on the Seebeck effect," *Sens. Actuators*, vol. 10, pp. 321–346, 1986.
- [29] F. Volklein and H. Baltes, "Thermoelectric properties of polysilicon films doped with phosphorous and boron," *Sens. Materials*, vol. 3, no. 6, pp. 325–224, 1992.
- [30] G. R. Lahiji and K. D. Wise, "A batch-fabricated silicon thermopile infrared detector," *IEEE Trans. Electron Devices*, vol. ED-29, pp. 14–22, Jan. 1982.
- [31] A. W. van Herwaarden, *Thermal Vacuum Sensors Based on Integrated Silicon Thermopiles*, Ph.D. thesis, Delft Univ. Technol., The Netherlands, 1987.
- [32] E. H. Kennard, *Kinetic Theory of Gases*. New York: McGraw-Hill, 1938, p. 314.
- [33] C. H. Mastrangelo, *Thermal Applications of Microbridges*, Ph.D. thesis, UC Berkeley and UMI Dissertation Services, 1991, Appendix II.
- [34] W. C. Tang, T.-C. H. Nguyen, M. W. Judy, and R. T. Howe, "Electrostatic-comb drive of lateral polysilicon resonators," *Sens. Actuators A*, vols. 21–23, pp. 328–331, 1990.
- [35] Y. Gianchandani and K. Najafi, "A bulk silicon dissolved wafer process for microelectromechanical devices," *J. Microelectromech. Syst.*, vol. 1, no. 3, pp. 77–85, June 1992.
- [36] R. I. Pratt, G. C. Johnson, R. T. Howe, and J. C. Chang, "Micromechanical structures for thin film characterization," in *Proc., Intl. Conf. on Solid-State Sensors and Actuators (Transducers '91)*, San Francisco, CA, June 1991, pp. 205–208.
- [37] F. Bordini and A. D'Amico, "Noise in sensors," *Sens. Actuators A*, vols. 21–23, pp. 17–24, 1990.
- [38] Y. Gianchandani and K. Najafi, "Batch-assembled multi-level micromachined mechanisms from bulk silicon," *J. Micromech. Microeng.*, vol. 2, pp. 80–85, 1992.
- [39] W. H. Juan and S. W. Pang, "A novel etch-diffusion process for fabricating high aspect ratio Si microstructures," in *Tech. Dig., 8th Int. Conf. Solid-State Sensors & Actuators (Transducers '95)*, Stockholm, Sweden, June 1995, pp. 560–563.
- [40] Y. B. Gianchandani, K. Ma, and K. Najafi, "A CMOS dissolved wafer process for integrated p<sup>++</sup> microelectromechanical systems," in *Tech. Dig., 8th Int. Conf. Solid-State Sensors & Actuators (Transducers '95)*, Stockholm, June 1995, pp. 79–82.
- [41] Y. B. Gianchandani and K. Najafi, "Bent-beam strain sensors," *J. Microelectromech. Syst.*, pp. 52–58, vol. 5, no. 1, Mar. 1996.
- [42] Y. Zhang and K. D. Wise, "Performance of nonplanar silicon diaphragms under large deflections," *J. Microelectromech. Syst.*, vol. 3, no. 2, pp. 59–68, June 1994.
- [43] K. Najafi and K. D. Wise, "An implantable multi-electrode array with on-chip signal processing," *IEEE J. Solid-State Circuits*, vol. 21, pp. 1035–1044, Dec. 1986.
- [44] K. Suzuki, K. Najafi, and K. D. Wise, "A 1024-element high-performance silicon tactile imager," *IEEE Trans. Electron Devices*, vol. 37, pp. 1852–1860, Aug. 1990.
- [45] S. T. Cho, K. Najafi, C. E. Lowman, and K. D. Wise, "An ultrasensitive silicon pressure-based microflow sensor," *IEEE Trans. Electron Devices*, vol. 39, pp. 825–835, Apr. 1992.
- [46] J. Bernstein, S. Cho, A. T. King, A. Kourpenis, P. Maciel, and M. Weinberg, "A micromachined comb-drive tuning fork rate gyroscope," in *Proc., IEEE Micro Electro Mechanical Systems Workshop (MEMS '93)*, Ft. Lauderdale, FL, Feb. 1993, pp. 143–148.
- [47] K. J. Ma, N. Yazdi, and K. Najafi, "A bulk silicon capacitive microaccelerometer with built-in overrange and force feedback electrodes," in *Dig. Solid-State Sensor and Actuator Workshop*, Hilton Head, SC, 1994.
- [48] J. K. Robertson and K. D. Wise, "A nested electrostatically-actuated microvalve for an integrated microflow controller," in *Proc., IEEE Workshop on Micro Electro Mechanical Systems (MEMS '94)*, Oiso, Japan, Feb. 1994, pp. 7–12.
- [49] J. Chen and K. D. Wise, "A high-resolution silicon monolithic nozzle array for inkjet printing," in *Tech. Dig., 8th Int. Conf. on Solid-State Sensors and Actuators (Transducers '95)*, Stockholm, Sweden, June 1995, pp. 321–324.



**Yogesh B. Gianchandani** (M'85–S'90–M'94) received the B.S. degree from the University of California, Irvine, in 1984, the M.S. degree from the University of California, Los Angeles, in 1986, and the Ph.D. degree from the University of Michigan, Ann Arbor, in 1994, all in electrical engineering.

His work at the Xerox Corporation from 1985 to 1988 and in Microchip Technology from 1988 to 1989 focused on the design of integrated circuits. From 1994 to August 1997, he was a Research Fellow in the Center for Integrated Sensors and Circuits at the University of Michigan, Ann Arbor. He is currently an Assistant Professor with the Department of Electrical and Computer Engineering, University of Wisconsin, Madison, WI. His research interests include all aspects of design, fabrication, and packaging of micromachined sensors and actuators and their interface circuits. His current emphasis is on technology development for the integration of MEMS with CMOS circuits. He has also contributed to the development of micromachined devices for inertial sensing, environmental sensing, scanning microscopy, material characterization, and biomedical applications.

Dr. Gianchandani is a member of Tau Beta Pi and Eta Kappa Nu.



**Khalil Najafi** (S'84–M'86) was born in 1958 in Iran. He received the B.S. degree in 1980 and the M.S. degree in 1981, and the Ph.D. degree in 1986, all in electrical engineering, from the Department of Electrical Engineering and Computer Science, University of Michigan, Ann Arbor.

From 1986 to 1988, he was employed as a Research Fellow, from 1988 to 1990, as an Assistant Research Scientist, from 1990 to 1993, as an Assistant Professor, and since September 1993, as an Associate Professor in the Center for Integrated Sensors and Circuits, Department of Electrical Engineering and Computer Science, University of Michigan. His research interests include: development of microfabrication and micromachining technologies for solid-state integrated sensors and microactuators; analog and digital integrated circuits; implantable microtelemetry systems and transducers for biomedical applications and wireless communication; technologies and structures for micro electromechanical systems (MEMS) and microstructures; hermetic packaging techniques for microtransducers; and low-power wireless sensing/actuating systems.

Dr. Najafi was awarded a National Science Foundation Young Investigator Award from 1992 to 1997, was the recipient of the Beatrice Winner Award for Editorial Excellence at the 1986 International Solid-State Circuits Conference, and of the Paul Rappaport Award for co-authoring the Best Paper published in the IEEE TRANSACTIONS ON ELECTRON DEVICES. In 1994, he received the University of Michigan's "Henry Russel Award" for outstanding achievement and scholarship, and was selected by students in the EECS Department as the "Professor of the Year" in 1993. He has been active in the field of solid-state sensors and actuators for more than ten years, and has been involved in the program committees of several conferences and workshops dealing with solid-state sensors and actuators, including the International Electron Devices Meeting, the Hilton-Head Solid-State Sensors and Actuators Workshop, and the IEEE/ASME Micro Electromechanical Systems (MEMS) Workshop. Dr. Najafi is the Editor for Solid-State Sensors for IEEE TRANSACTIONS ON ELECTRON DEVICES, and an Associate Editor for the *Journal of Micromechanics and Microengineering*, Institute of Physics Publishing.